

Dual In-painting Model for Unsupervised Gaze Correction and Animation in the Wild

Jichao Zhang¹, Jingjing Chen², Hao Tang¹, Wei Wang³, Yan Yan⁴, Enver Sangineto¹, Nicu Sebe^{1,5}

¹University of Trento, ²Shandong University, ³École Polytechnique Fédérale de Lausanne

⁴Texas State University, ⁵Huawei Research Ireland

ABSTRACT

In this paper we address the problem of unsupervised gaze correction in the wild, presenting a solution that works without the need for precise annotations of the gaze angle and the head pose. We have created a new dataset called CelebAGaze, which consists of two domains X , Y , where the eyes are either staring at the camera or somewhere else. Our method consists of three novel modules: the Gaze Correction module (GCM), the Gaze Animation module (GAM), and the Pretrained Autoencoder module (PAM). Specifically, GCM and GAM separately train a dual in-painting network using data from the domain X for gaze correction and data from the domain Y for gaze animation. Additionally, a Synthesis-As-Training method is proposed when training GAM to encourage the features encoded from the eye region to be correlated with the angle information, resulting in a gaze animation which can be achieved by interpolation in the latent space. To further preserve the identity information (e.g., eye shape, iris color), we propose the PAM with an Autoencoder, which is based on Self-Supervised mirror learning where the bottleneck features are angle-invariant and which works as an extra input to the dual in-painting models. Extensive experiments validate the effectiveness of the proposed method for gaze correction and gaze animation in the wild and demonstrate the superiority of our approach in producing more compelling results than state-of-the-art baselines. Our code, the pretrained models and the supplementary material are available at: <https://github.com/zhangqianhui/GazeAnimation>.

CCS CONCEPTS

• **Computing methodologies** → *Computational photography; Image representations.*

KEYWORDS

Deep Learning, Generative Adversarial Networks, Image Translation, Gaze Correction, Gaze Animation

ACM Reference Format:

Jichao Zhang¹, Jingjing Chen², Hao Tang¹, Wei Wang³, Yan Yan⁴, Enver Sangineto¹, Nicu Sebe^{1,5}. 2020. Dual In-painting Model for Unsupervised Gaze Correction and Animation in the Wild. In *Proceedings of the 28th ACM International Conference on Multimedia (MM '20)*, October 12–16, 2020,

Permission to make digital or hard copies of all or part of this work for personal or classroom use is granted without fee provided that copies are not made or distributed for profit or commercial advantage and that copies bear this notice and the full citation on the first page. Copyrights for components of this work owned by others than ACM must be honored. Abstracting with credit is permitted. To copy otherwise, or republish, to post on servers or to redistribute to lists, requires prior specific permission and/or a fee. Request permissions from [permissions@acm.org](https://permissions.acm.org).

MM '20, October 12–16, 2020, Seattle, WA, USA

© 2020 Association for Computing Machinery.

ACM ISBN 978-1-4503-7988-5/20/10...\$15.00

<https://doi.org/10.1145/3394171.3413981>

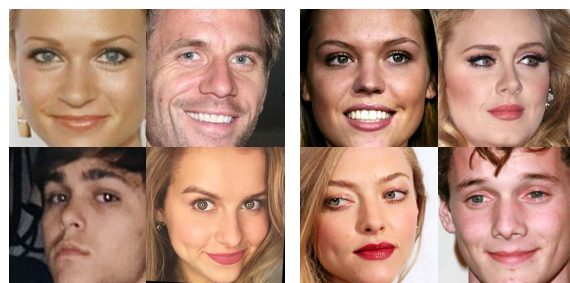


Figure 1: A few example images of the CelebAGaze dataset. Left: People staring at the camera for domain X . Right: People staring somewhere else for domain Y . These examples show the diversity in the head pose, the gaze angle and the illumination conditions of the proposed dataset.

Seattle, WA, USA. ACM, New York, NY, USA, 12 pages. <https://doi.org/10.1145/3394171.3413981>

1 INTRODUCTION

Gaze correction aims at manipulating the eye gaze with respect to the desired direction. This is important in some real-life scenarios where there is the need to “move” the person’s gaze into the camera. For example, shooting a good portrait is challenging as the subject may be too nervous to stare at the camera. Another scenario is videoconferencing where the eye contact is extremely important as the gaze can express attributes such as attentiveness and confidence. Unfortunately, eye contact and gaze awareness are lost in most videoconferencing systems, as the participants look at the monitors and not directly into the camera.

Early works in gaze correction relied on special hardware, such as stereo cameras [3, 46], Kinect sensor [21] or transparent mirrors [18, 30]. Recently, some learning-based methods have produced very high-quality synthetic images with a corrected gaze. For instance, Kononenko and Lempitsky [20] propose to solve the problem of monocular gaze correction using decision forests. DeepWarp [6] uses a deep network to directly predict an image-warping flow field with a coarse-to-fine learning process. However, despite its good qualitative results, this method fails in generating photo-realistic images when redirecting the gaze for large angles. Additionally, it produces unnatural eye shapes as the $L1$ loss is exploited to learn the flow field without any geometry regularization. To solve this problem, PRGAN [9] proposes to exploit adversarial learning with a cycle-consistent loss to generate more plausible gaze redirection results. However, it is challenging for these methods [6, 9, 20] to obtain high-quality gaze redirection results in the wild when there are large variations in the head pose, gaze angles *etc.* Another category of works is based on a 3D model without training data such as GazeDirector [44]. The main idea of GazeDirector is to

model the eye region in a 3D reference system instead of predicting a flow field directly from the input image. However, modeling in 3D has strong assumptions that do not hold in reality.

More importantly, the previous methods need training labels of the head pose and gaze angles, but these are hard to obtain in the wild. To solve these problems, we collected the CelebAGaze dataset which consists of two domains: eyes staring at the camera for domain X and eyes staring somewhere else for domain Y , as shown in Fig. 11. Note that no paired samples exist in the CelebAGaze dataset. We propose an unsupervised learning method for gaze correction and animation consisting of three modules: 1) GCM is an in-painting model, trained on the domain X , which learns how to fill in the missing eye regions with the new content which has the corrected eye gaze; 2) GAM exploits the other in-painting model, trained on the domain Y . To generalize the gaze animation with various angle directions, we propose the Synthesis-As-Training method to use synthesizing data for training GAM, encouraging the features encoded from the eye region to be corrected with the angle information. Finally, gaze animation can be achieved by interpolating this feature in the latent space; 3) PAM encodes the angle-invariant content features, e.g., iris color, eye shape. Specifically, we pretrain an autoencoder by self-supervised mirror learning where the bottleneck features are extracted as an extra input of the dual in-painting model to preserve the identity of the corrected results. Finally, both the qualitative and quantitative evaluations demonstrate that our model achieves more compelling results than the state-of-the-art baselines in gaze correction and gaze animation. To recap, our main contributions are:

- 1) We propose a simple yet effective dual in-painting method for gaze correction and animation.
- 2) For gaze animation, we introduce a novel Synthesis-As-Training Method which encourages the features encoded from the eye region to be correlated with the angle information.
- 3) We design a novel Self-Supervised Mirror Learning for pretraining an autoencoder to extract content features to preserve the identity of the corrected results.
- 4) We make available to the research community a new gaze dataset for gaze correction and animation.

2 RELATED WORK

Generative Adversarial Networks: Generative Adversarial Networks [7] are powerful generative models which learn a distribution that mimics a given target distribution. They have been applied to many fields, such as low-level image processing tasks (image in-painting [12, 36], image super-resolution [22, 23, 42]), high-level semantic and style transfer (image translation [14, 26, 28, 33, 40, 41, 55], person image synthesis [38, 39], image manipulation [34]).

Image Inpainting: Image inpainting, an important task in computer vision and graphics, aims at filling the missing pixels of an image with plausibly synthetic content. Recently, CNN-based and GAN-based methods have shown promising performance on image inpainting [13, 24, 35, 50]. Thus, some works try to apply an inpainting model for facial attribute manipulation, such as hair, mouth and eye [4, 15, 31]. Similar to these methods, our approach also follows the deep inpainting methods, but it does not require

the data to be labeled or other additional information, such as a semantic segmentation mask, a sketch and even a reference image.

Gaze Correction: Previous work for gaze correction can be divided into three classes: 1) hardware-driven, 2) rendering and synthesis, 3) learning-based.

The hardware support is indispensable in early research. Kolarits *et al.* [18] tried to make use of half-silvered mirrors to allow the camera to be placed on the optical path of the display. Yang *et al.* [47] aimed to address the eye contact problem with a novel view synthesis, and they use a pair of calibrated stereo cameras and a face model to track the head pose in 3D. Generally speaking, these hardware-based methods are expensive.

Some works render the eye region based on a 3D fitting model, which replaces the original eye with new synthetic eyeballs. Banf *et al.* [1] uses an example-based approach for deforming the eyelids and slide the iris across the model surface with texture-coordinate interpolation. To fix the limitation caused by the use of a mesh, where the face and eyes are joined, GazeDirector [44] regards the face and eyeballs as separate parts, synthesizing more high-quality images, especially for large redirection angles. These methods can be applied to eye correction, but they struggle when rendering eyes realistically is a challenge. Additionally, modeling methods have strong assumptions that usually do not hold in reality.

The core idea for most of the learning-based methods is to use a large paired training dataset to train the model [19, 20, 32, 48]. Some methods [19, 20] learn to generate the flow field which is used to relocate the eye pixels in the original image. Ganin *et al.* [6] proposes to use a convolutional network to learn the flow field warping the input image for redirecting the gaze to the desired angle. However, the model fails to generate photo-realistic and natural shape results of gaze redirection, as it uses only pixel-wise differences between the input and the ground truth as the loss. To solve this problem, He *et al.* [9] propose to use adversarial learning jointly with a cycle-consistent loss, which can improve the visual quality and redirection precision. However, these methods can hardly generate plausible results in the wild, coping with large variations in head pose, gaze angle and illumination. In contrast, we propose to utilize an in-painting model to correct the gaze angle which can generate high-quality gaze correction and gaze animation in the wild.

3 METHOD

The overview of our method is shown in Fig. 2 and it consists of three modules: the Gaze correction Module (GCM), the Gaze Animation Module (GAM) and the Pretrained Autoencoder Module (PAM). Before introducing the details, we first clarify the notation.

- $z \in Z$ indicates an image instance represented in $Z = R^{m \times n \times c}$, where m, n, c are the height, the width and the number of channels.

- Z is divided into two domains: X containing image instances with gaze staring at the camera and Y containing image instance with gaze staring somewhere else.

- $M \in R^{m \times n \times c}$ denotes a binary mask of the eye region and M' defines the operation of extracting a sub-image (eye region) for a rectangular region.

- P_x, P_y denote distributions of data from the domains X and Y , respectively. P_m denotes the distribution of data $M(z)$ with the eye regions removed. $M(x)$ and $M(y)$ have the same distribution,

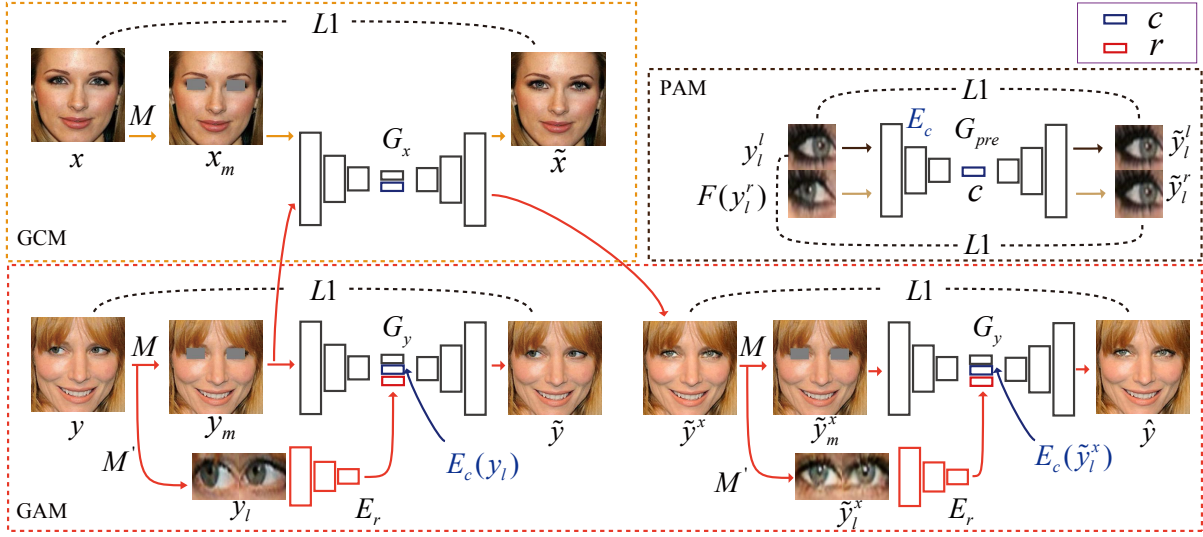


Figure 2: An overview of our method. In GCM, G_x uses x from domain X for training. In GAM, G_y uses y from domain Y for training. Compared to G_x , G_y has an extra encoder (E_r) to extract a feature r (marked with a red box) as input. We use G_x to get the corrected result \tilde{y}^x which is used for training G_y (Synthesis-As-Training Method). For PAM, G_{pre} is trained using the left (or right) eye y_l^l and the flipping result $F(y_l^r)$ of the right (or left) eye y_l^r to learn angle-invariant content features c (marked with a blue box). The encoder of G_{pre} is used in dual in-painting models to extract the feature r as an extra input. We then compute pixel-wise differences with the $L1$ loss to optimize G . Note that the adversarial loss and the reconstruction loss are also used, but they are not shown in this figure.

as the images $x \in X$ and $y \in Y$ have the only discrepancy in the eye region. Thus, $M(x) \sim P_m$, $M(y) \sim P_m$.

- $r \in \mathbb{R}^2$, $c \in \mathbb{R}^{256}$ denote the angle and the content features (angle-invariant) where both are extracted by different encoders.
- F denotes the image horizontal flipping operation (Mirroring).

3.1 GCM with Generator G_x

As shown in Fig. 2, G_x is trained on data x from domain X and it aims to complete the masked image $x_m = M(x)$ by synthesizing the eye region. In theory, G_x can learn the mapping from P_m to P_x , thus, $\tilde{x} = G_x(M(x))$ and $\tilde{y}^x = G_x(M(y))$. Then, $\tilde{x} \sim P_x$, $\tilde{y}^x \sim P_x$, as $M(x)$ and $M(y)$ have the same distribution P_m . This is the theoretical basis of our correction module. Specifically, we can use G_x to correct the gaze to stare at the camera for data y from domain Y . It can be represented as:

$$\begin{aligned} c_x &= E_c(M'(x)), c_y = E_c(M'(y)) \\ \tilde{x} &= G_x(M(x), c_x), \tilde{y}^x = G_x(M(y), c_y), \end{aligned} \quad (1)$$

where c_x and c_y are the content features encoded from $M'(x)$ and $M'(y)$ by E_c . E_c is the encoder of G_{pre} which will be introduced in Section 3.3.

We use a pixel-wise loss ($L1$) for training GCM, shown in Fig. 2. It is defined as:

$$\ell_{recon}^x = \mathbb{E}_{x \sim P_x} [\|x - \tilde{x}\|_1]. \quad (2)$$

3.2 GAM with Generator G_y

In addition to correct the gaze to stare at the camera, it is more valuable and efficient to redirect the gaze into any direction for gaze animation. Thus, we propose a novel Synthesis-As-Training Method, in which we use the synthetically corrected data as training data of the other generator G_y to learn gaze animation.

In detail, this module can be divided into two stages. In the first stage we train the inpainting model G_y to fill-in the masked image $y_m = M(y)$ and produce \tilde{y} . Different from G_x , G_y encodes the eye region into the latent code $r \in \mathbb{R}^2$ by exploiting E_r , where r is an extra input of the decoder in G_y .

$$\begin{aligned} r_y &= E_r(M'(y)), c_y = E_c(M'(y)) \\ \tilde{y} &= G_{y \sim P_y}(M(y), r_y, c_y). \end{aligned} \quad (3)$$

The reconstruction loss for PAM is defined as:

$$\ell_{recon}^y = \mathbb{E}_{y \sim P_y} [\|y - \tilde{y}\|_1]. \quad (4)$$

In the second stage, we use G_x to correct the gaze of y and produce the synthetic sample \tilde{y}^x with the corrected gaze, shown in the right side of Fig. 2. Then, \tilde{y}^x is used for training G_y , just like y does. With the paired samples (y, \tilde{y}^x) , which have the same incomplete region $M(y)$ but different eye region (i.e., y_l, \tilde{y}_l^x), we train GAM and we ensure that the encoded feature r has a highly correlation with the gaze angle.

$$\begin{aligned} r_{\tilde{y}^x} &= E_r(M'(\tilde{y}^x)), c_{\tilde{y}^x} = E_c(M'(\tilde{y}^x)) \\ \hat{y} &= G_y(M(\tilde{y}^x), r_{\tilde{y}^x}, c_{\tilde{y}^x}). \end{aligned} \quad (5)$$

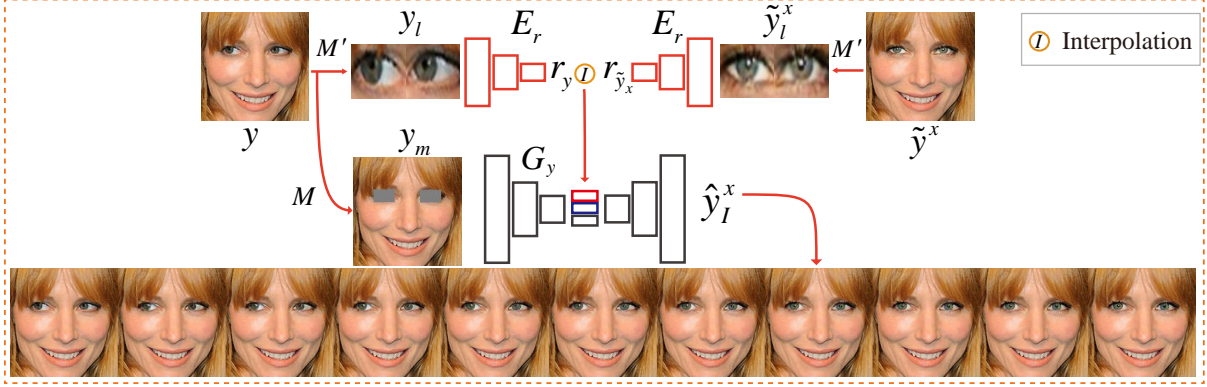


Figure 3: An overview of the architectures of our networks for gaze animation. r_y and $r_{\tilde{y}^x}$ are the angle representation of the input image y and the corrected result \tilde{y}^x , respectively. The bottom figure shows the interpolation process between r_y and $r_{\tilde{y}^x}$, where the new angle representation is fed to G_y to obtain the final output \hat{y}_l^x .

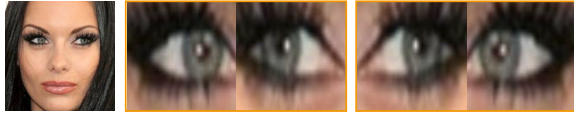


Figure 4: Training samples in PAM. The first column is the input image y . The other columns show (from left to right): the left eye (y_l^l), the flipping result of right eye ($F(y_l^r)$), the right eye (y_l^r), and the flipping result of left eye ($F(y_l^l)$).

The corresponding loss is defined as:

$$\ell_{recon}^{\tilde{y}^x} = \mathbb{E}_{y \sim P_y} [\|\tilde{y}^x - \hat{y}\|_1]. \quad (6)$$

We exploit $\ell_{recon}^y + \ell_{recon}^{\tilde{y}^x}$ as objective functions for training E_r and G_y . And we interpolate this feature r between $E_r(y_l)$ and $E_r(\tilde{y}_l^x)$ to produce the gaze animation which will be introduced later.

3.3 PAM with Self-Supervised Mirror Learning

This inpainting process has difficulties in preserving the consistency of the identity information (e.g., iris color, eye shape). Consequently, we propose to pretrain G_{pre} to learn the content features (c). Then, c is used as the guidance for G_x and G_y to preserve the identity information of the inpainted results (c denoted with a blue box in Fig. 2).

Although our training dataset is collected from the Internet, the majority of the images it is composed of, are close to the frontal image (first column in Fig. 4). As shown in columns 2-5 of Fig. 4, we have paired images: left eye y_l^l and the mirror $F(y_l^r)$ of the right eye y_l^r , where both have different angles, but they have a very similar eye shape, iris color, etc., likewise for y_l^r . Based on this observation, as shown in the top-right of Fig. 2, we use two paired samples to pretrain G_{pre} using the following objective functions:

$$\begin{aligned} \ell_{pre} = & \mathbb{E}_{y \sim P_y} [\|y_l^l - G_{pre}(y_l^l)\|_1 + \|y_l^l - G_{pre}(F(y_l^r))\|_1 \\ & + \|y_l^r - G_{pre}(y_l^r)\|_1 + \|y_l^r - G_{pre}(F(y_l^l))\|_1]. \end{aligned}$$

After training, we found that the bottleneck feature c of G_{pre} is quasi angle-invariant, containing only the content information (iris color, eye shape). Thus, we use the encoder network E_c of G_{pre} as extra input of G_x and G_y to extract content features. With these features as guidance, the inpainted results are more consistent with the input in identity information.

3.4 Global and Local Discriminators for Adversarial Learning

Since the L_1 loss tends to produce blurry results, we use two discriminators D_x and D_y adversarially trained. D_x , D_y do not share the weights of all the layers. Moreover, inspired by [13], we use a global discriminator that takes the entire face as input and a local discriminator which takes the local eye region as input. The global part is used to make coherent the entire image as a whole, while the local part is used to make the local region more realistic and sharper. We concatenate the final fully-connected feature map of both parts into one output which is used as the input of a sigmoid function to predict the probability of the image being real. The objective function for D_x and G_x is defined as:

$$\begin{aligned} \min_{G_x} \max_{D_x} \ell_{adv}^x = & \mathbb{E}_{x \sim P_x} [\log D_x(x, M'(x))] \\ & + \mathbb{E}_{x \sim P_x} [\log(1 - D_x(\tilde{x}, M'(\tilde{x})))] \\ & + \mathbb{E}_{y \sim P_y} [\log(1 - D_x(\tilde{y}, M'(\tilde{y})))] \quad (7) \end{aligned}$$

The objective function for D_y and G_y is defined as:

$$\begin{aligned} \min_{G_y} \max_{D_y} \ell_{adv}^y = & \mathbb{E}_{y \sim P_y} [\log D_y(y, M'(y))] \\ & + \mathbb{E}_{y \sim P_y} [\log(1 - D_y(\tilde{y}, M'(\tilde{y})))] \quad (8) \end{aligned}$$

3.5 Overall Loss

Similar to [11], we use a reconstruction loss for the content features in the latent space to further preserve the identity information between the input image and the corrected output. This loss (ℓ_{fp}) is defined as:

$$\ell_{fp} = \mathbb{E}_{y \sim P_y} [\|r_y - E_r(M'(\tilde{y}))\|_1 + \|r_{\tilde{y}^x} - E_r(M'(\tilde{y}^x))\|_1]. \quad (9)$$

We use $-\ell_{adv}^x$ to train D_x and $-\ell_{adv}^y$ to train D_y . Concerning G_x , the overall loss is defined as:

$$\ell_{all}^x = \ell_{adv}^x + \lambda_1 \ell_{recon}^x. \quad (10)$$

For G_y and E_r , the overall loss is defined as:

$$\ell_{all}^y = \ell_{adv}^y + \lambda_2 \ell_{adv}^x + \lambda_3 \ell_{recon}^y + \lambda_4 \ell_{recon}^{\tilde{y}^x} + \lambda_5 \ell_{fp}, \quad (11)$$

where $\lambda_1, \lambda_2, \lambda_3, \lambda_4$ and λ_5 are hyper-parameters controlling the contributions of each loss term.

3.6 Inference for Gaze correction and Animation

We obtain the correction result \tilde{y}^x for a given sample y using G_x . As shown in Fig. 3 (top), we modify the encoded representation r by interpolating between r_y and $r_{\tilde{y}^x}$, which are encoded from the eye region y_l and \tilde{y}_l^x , respectively. The new representation can be fed to G_y to obtain animation results \hat{y}_l^x with different angles. As shown in the bottom of Fig. 3, we obtain plausible and smooth gaze animations in the wild.

4 EXPERIMENTS

In this section, we first introduce the details of our dataset, the network training and the baseline models. Then, we compare the proposed method with the state-of-the-art methods on gaze correction in the wild using both qualitative and quantitative evaluations. Next, we demonstrate the effectiveness of the proposed method on gaze animation with various outputs by interpolating and extrapolating in the latent space. Finally, we present an ablation study to validate the effect of each component of our model, *i.e.*, Synthesis-As-Training Method, Pretrained Autoencoder with Self-Supervised Mirror Learning, and Latent Reconstruction Loss. For brevity, we refer to our full method as **GazeGAN**. *Note that we do not use any post-processing algorithm for GazeGAN.*

4.1 Dataset

CelebAGaze Dataset: Most of the existing benchmark datasets [5, 37, 53, 54] are not suitable for our gaze correction task in the wild, which asks for a wider gaze range, various head poses and different illumination conditions. Recently, [16] presented a large scale gaze tracking dataset, called Gaze360, for robust 3D gaze estimation in unconstrained images. Although this dataset has been labeled with a 3D gaze with a wide range of eye angles and head poses, it still lacks high-resolution images for face and eye regions. Additionally, this dataset does not provide the eye data with staring at the camera, which is required by our proposed unsupervised method.

To remedy this problem, we collected a new dataset, called CelebAGaze. In detail, CelebAGaze consists of 25283 high-resolution celebrity images that are collected from CelebA [27] and the Internet. It consists of 21832 face images with eyes staring at the camera and 3451 face images with eyes staring somewhere else. We cropped all images (256×256) and compute the eye mask region by dlib [17]. Specifically, we use dlib to extract 68 facial landmarks and calculate the mean of 6 points near the eye region, which will be the center point of the mask. The size of the mask is fixed to 30×50 . As described above, we randomly select 300 samples from domain Y , 100 samples from domain X as the test set, the remaining as the

Table 1: Columns 1-2: the MSSSIM and LPIPS scores computed on the background regions of the gaze correction results using different models. Column 3: the user study results. Higher is better for MSSSIM and the user study; lower is better for LPIPS.

Metrics	MSSSIM \uparrow	LPIPS \downarrow	User Studies \uparrow
Other	-	-	24.20%
StarGAN [2]	0.969	0.0732	3.40 %
StarGANA	0.998	0.0022	6.67 %
CycleGAN [55]	0.991	0.0267	15.00 %
PRGAN [9]	1.0	0.0	8.33 %
GazeGAN	1.0	0.0	42.40 %
GT	1.0	0.0	100%

training set. Note that this dataset is unpaired and it is not labeled with the specific eye angle or the head pose information. We show some samples of the CelebAGaze dataset in Fig. 11.

4.2 Training Details

We first train the PAM module. Then, the discriminators D_x and D_y and the generators G_x and G_y are jointly optimized. We use the Adam optimizer with $\beta_1 = 0.5$ and $\beta_2 = 0.999$. The batch size is 8. The initial learning rate for PAM is 0.0005 and 0.0001 for the discriminators and the generators in the first 20000 iterations, and linearly decayed to 0 over the remaining iterations. All the weight coefficients $\lambda_1, \lambda_2, \lambda_3, \lambda_4, \lambda_5$ are set to 1. To stabilize the network training in the adversarial learning, we use spectral normalization [29] for all the convolutional layers of the discriminators D_x and D_y , but not for the generator G_x . Our model is implemented in Tensorflow and takes ten hours to be trained with a single NVIDIA Titan X GPU.

4.3 Baseline Models

Gaze Correction: PRGAN [9] achieved state-of-the-art gaze redirection results on the Columbia dataset based on a single encoder-decoder network with adversarial learning, similarly to StarGAN [2]. The original PRGAN is trained on paired samples with labeled angles (Columbia Gaze [37]). To train PRGAN on the proposed CelebAGaze dataset, we remove the VGG perceptual loss of PRGAN and learn the domain translation between X and Y . Note that we train PRGAN only with the local eye region, the same way as in the original paper.

Facial Attribute Manipulation: Gaze correction and animation can be regarded as a sub-task of facial attribute manipulation. Recently, StarGAN [2] achieved very high-quality results in facial attribute manipulation. We train StarGAN on the CelebAGaze dataset to learn the translation mapping between domain X and domain Y . To further improve the ability of StarGAN on this task, we employ a variant of StarGAN as an additional baseline: StarGAN with spatial attention learning [49] referred to as StarGANA. Moreover, gaze correction can be considered as an image translation task. Thus, we adopt CycleGAN as another baseline for our experiments. Note that we do not compare GazeGAN with SGGAN [51], AttGAN [10],

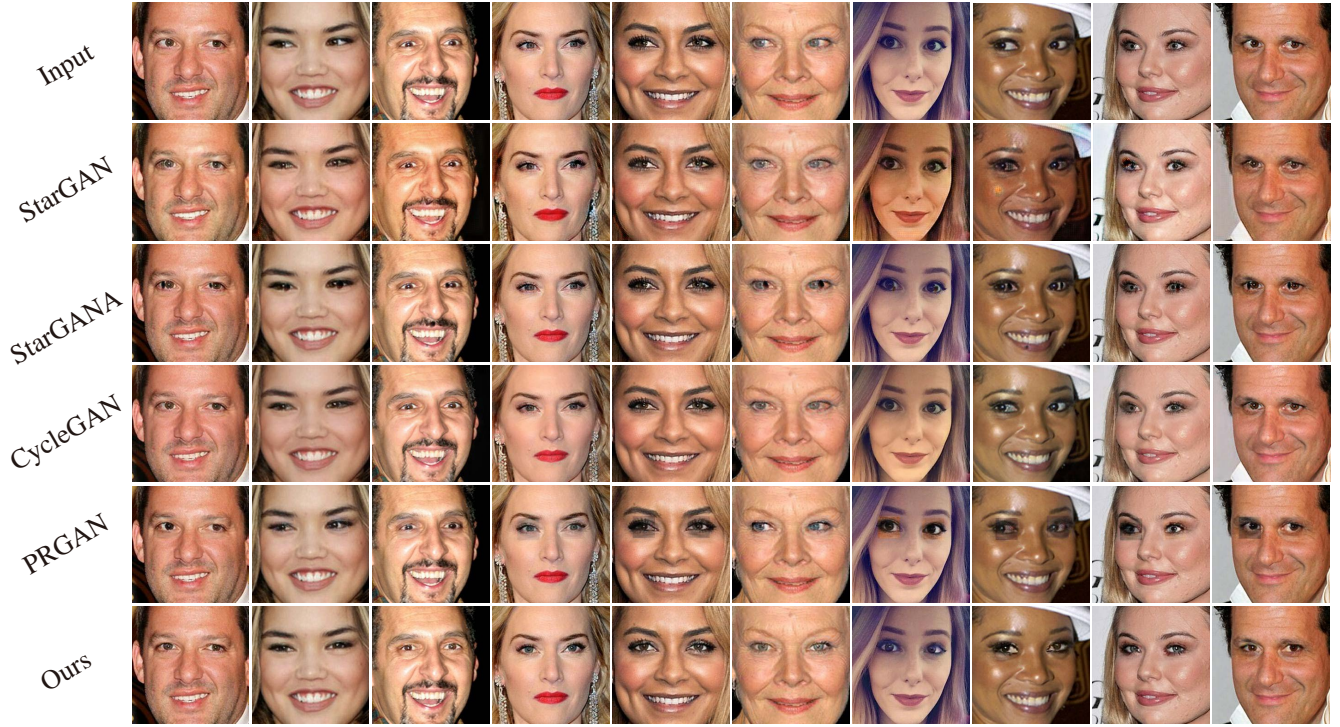


Figure 5: Qualitative comparison for the gaze correction task. The first row shows the input images and the following rows show the gaze correction results of StarGAN [2], StarGANA, CycleGAN [55], PRGAN [9] and GazeGAN.

STGAN [25], RelGAN [45] and PAGAN [8], as they have a performance very close to StarGAN in facial attribute manipulation. We use the public code of StarGAN ¹, CycleGAN ² and PRGAN ³.

4.4 Gaze correction

In this section, we first qualitatively compare the proposed method with state-of-the-art methods on the CelebAGaze dataset for the task of gaze correction. Then, we choose some metrics to quantitatively evaluate the gaze correction results.

Qualitative results: As shown in the last row of Fig. 5, GazeGAN can correct the eyes to look at the camera while preserving the identity information such as the eye shape and the iris color, validating the effectiveness of the proposed method. The 2nd row shows the results of StarGAN [2]. We note that StarGAN could not produce precise gazes staring at the camera and it suffers for the low-quality generation with lots of artifacts. The results of CycleGAN are shown in 4th row. Although the results of CycleGAN are very realistic and with low artifacts in the eye region, this method does not produce a precise correction for the gaze. We believe that this is because both StarGAN and CycleGAN are based on the cycle-consistency loss, which requires that the mapping between X and Y should be continuous and invertible. According to the invariance of the Domain Theorem ⁴, the intrinsic dimensions

of the two domains should be the same. However, the intrinsic dimension of Y is much larger than X , as Y has more variations for the gaze angle than X . As shown in the 7th columns of Fig. 5, both StarGAN and CycleGAN cannot preserve the irrelevant regions of the face. Another stronger baseline is StarGANA, which combines spatial attention [49] with StarGAN, and successfully preserves the irrelevant region (shown in the 3rd row). However, the results of StarGANA are not faithfully and realistic, with lots of deformation artifacts, compared with GazeGAN.

Moreover, we compare GazeGAN with PRGAN [9], which is trained using only local eye regions (same as in the original paper), which may be helpful to focus on the translation in the eye region. The results of PRGAN are shown in the 5th row of Fig. 5. Compared with GazeGAN, PRGAN does not produce precise and realistic correction results, similarly to StarGAN and CycleGAN. Additionally, PRGAN suffers from the boundary mismatch problem between the local eye region and the global face.

Quantitative Evaluation Protocol: The qualitative evaluation has validated the effectiveness and the superiority of our proposed GazeGAN in gaze correction. To further support the previous evaluation with a quantitative evaluation, we employ MSSSIM [43] and LPIPS [52] to measure the *preservation* ability of the *irrelevant regions*, i.e., faces without the eye region ($M(y)$). Specifically, we compute the mean MSSSIM and LPIPS scores between $M(y)$ and $M(\hat{y})$ across all the test data from domain Y .

In addition to the metrics aforementioned, we conduct a user study to assess the results of the gaze correction from different

¹<https://github.com/yunjey/StarGAN>

²<https://github.com/junyanz/pytorch-CycleGAN-and-pix2pix>

³https://github.com/HzDmS/gaze_redirection

⁴https://en.wikipedia.org/wiki/Invariance_of_domain

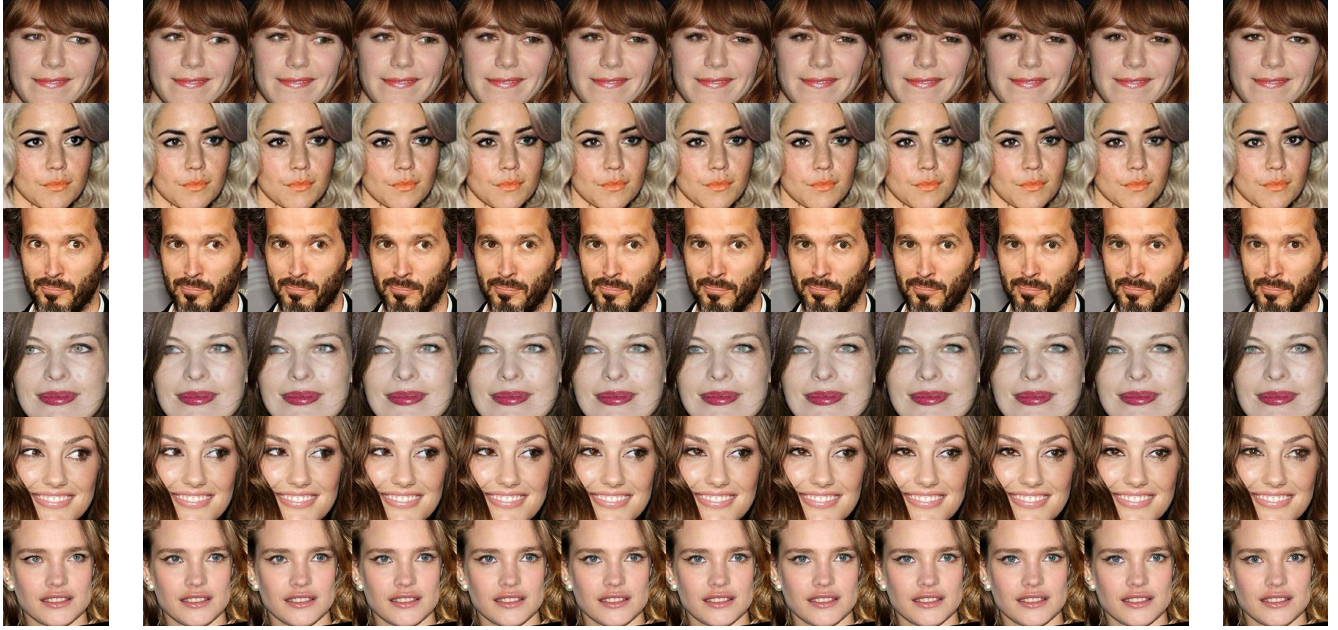


Figure 6: Gaze animation results using the interpolation of the latent features r . The first and the final column show the input images and corrected results, respectively. The middle columns show the interpolated images.



Figure 7: Gaze animation examples obtained by both interpolation and extrapolation of the latent features r . The 1st row shows the interpolation results and the next two rows show the extrapolation results.

models. In detail, given an input face image in the CelebAGaze test dataset (extracted from Y), we show the corrected results from different models to 30 respondents who were asked to select the best image based on perceptual realism and the precision of the gaze correction. They also can select “Other” which means that the results from all the models are not satisfactory. This study is based on 50 questions for all respondents.

Quantitative results: The first two columns of Table 1 show the MSSSIM and LPIPS scores evaluating the preservation ability of the corrected images across different models. GazeGAN and PRGAN obtain the best results with 1.0 for MSSSIM and 0.0 for

Table 2: Comparison between GazeGAN and GazeGAN W/O A , where the latter denotes removing the content representation extracted from E_c . The scores are measured between the input image x and inpainted result \tilde{x} across all the test data from X .

Metrics	GazeGAN	GazeGAN W/O A
MSSSIM \uparrow	0.67	0.52
LPIPS \downarrow	0.1680	0.2410

Table 3: Comparison with GazeGAN W/O C , which denotes removing the latent reconstruction loss ℓ_{fp} . The scores are measured between the input image y and the reconstruction result \tilde{y} across all the test data from Y .

Metrics	GazeGAN	GazeGAN W/O C
MSSSIM \uparrow	0.59	0.53
LPIPS \downarrow	0.2506	0.2675

LPIPS. In fact, the original irrelevant regions are integrated with the generated eye region in both models using binary masks. StarGAN, StarGANA and CycleGAN obtain the worse irrelevant region preservation scores. The last column of Table 1 shows the evaluation results of the user study. The user average vote for GazeGAN is 42.40%, which is higher than all the other methods, *i.e.*, 3.40% higher than StarGAN, 6.67% higher than StarGANA, 15.00% higher than CycleGAN, 8.33% higher than PRGAN. Overall, the qualitative and quantitative evaluations demonstrate the effectiveness and the superiority of the proposed approach.

4.5 Gaze Animation

In Fig. 6 we show the gaze animation results using input images with an arbitrary gaze which are corrected to stare at the camera.

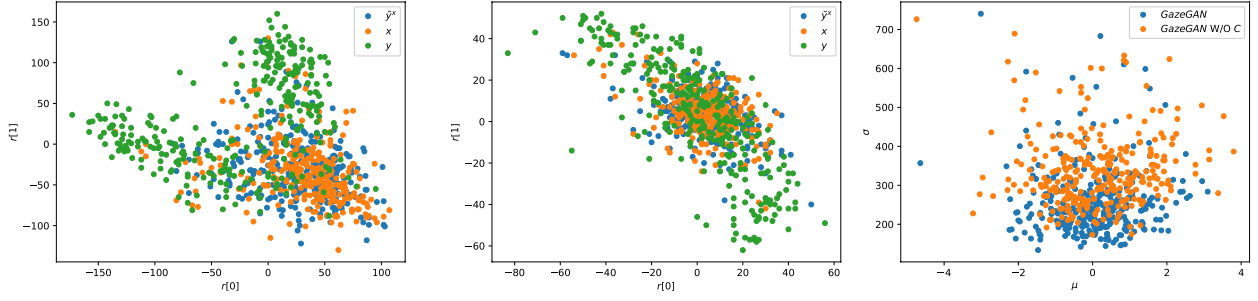


Figure 8: A visualization of the angle (columns 1-2) and the content (column 3) representations. Columns 1-2 correspond to the results of GazeGAN W/O B and GazeGAN, respectively. $r[0]$ and $r[1]$ mean the 1st and 2nd value of the r feature vector, respectively. Column 3 shows the mean (X-coordinate) and the variance (Y-coordinate) of the content representation differences between GazeGAN W/O C and GazeGAN.

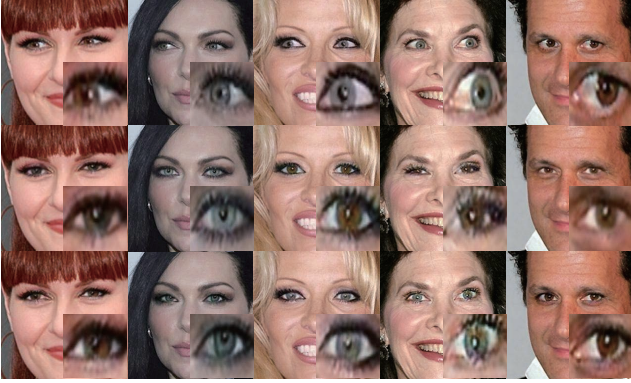


Figure 9: A qualitative comparison between GazeGAN and GazeGAN W/O A. The first row shows the input images and next two rows are the corrected results of GazeGAN W/O A and GazeGAN (Zoomed left eyes).

We observe that the interpolation results are smooth and plausible in each row. Each column has a different gaze angle, but the identity information is overall preserved (e.g., the eye shape, the iris color). Next, we show gaze animation results with more various directions by *extrapolating* the features r , in addition to interpolation methods. As shown in Fig. 7, our model not only achieves high-quality interpolation results but also achieves gaze animation with more directions where the angles are out of the range between the input and corrected output.

4.6 Ablation Study

In this section, we conduct extensive ablation studies to investigate the three key components of the proposed GazeGAN, i.e., the Pretrained Autoencoder for content extraction, the Synthesis-As-Training Method, and the Latent Reconstruction Loss ℓ_{fp} . For brevity, we refer to these components as A, B and C, respectively.

Pretrained Autoencoder: We propose this pretrained model to extract the content features to guide the process of gaze correction while preserving the identity information. We observe that GazeGAN has a stronger ability to preserve identity information

with respect to GazeGAN W/O A in Fig. 9. To quantitatively evaluate this, we use G_x to reconstruct the input image x from the test dataset in the domain X and we measure the differences between the input images and the correction results in the local eye regions by employing MSSSIM and LPIPS. Table 2 shows that GazeGAN achieves better scores than GazeGAN W/O A, validating our design motivation.

Training-As-Synthesis Method: The results in Fig. 6 have shown the effectiveness of this method for gaze animation. Additionally, we illustrate three groups of features r extracted from E_r with real test samples y , real test samples x , the corrected results \tilde{y}^x as input. In Fig. 8, the 1st and the 2nd column correspond to the results of GazeGAN W/O B, and GazeGAN respectively. We observe that the points corresponding to \tilde{y}^x are closer to the points corresponding to x in the 2nd figure with respect to what happens in the 1st column, which indicates that features r have a strong correlation with angle information.

Latent Reconstruction Loss ℓ_{fp} : We use G_y to complete the input images y from the test data of Y and we measure the differences between the input images and the results using MSSSIM and LPIPS. In Fig. 3, GazeGAN obtains higher scores than GazeGAN W/O C, which shows that ℓ_{fp} further improves the ability to preserve identity information. Additionally, we visualize the mean μ (X-coordinate) and the variance σ (Y-coordinate) of the arithmetical differences $c^{\tilde{y}} - c^y$ extracted from G_c across all the test data from Y. As shown in the right of Fig. 8, we see that our full model GazeGAN has a lower variance than GazeGAN W/O C, as the loss encourages to reduce the differences of the content features.

5 CONCLUSION

In this paper we introduced a new gaze dataset in the wild, CelebAGaze, which is characterized by a large diversity in the head poses, gaze angles and illumination conditions. Moreover, we presented a novel unsupervised model, GazeGAN, for gaze correction and animation, trained and tested on this dataset. GazeGAN generates more high-quality and precise gaze correction results than state-of-the-art methods. Furthermore, it can redirect the gaze into the desired direction, producing gaze animation by interpolation in the latent space. Future work includes extending the proposed model to gaze redirection tasks in videos.

REFERENCES

- [1] Michael Banf and Volker Blanz. 2009. Example-based rendering of eye movements. In *Computer Graphics Forum*, Vol. 28. Wiley Online Library, 659–666.
- [2] Yunje Choi, Minje Choi, Munyoung Kim, Jung-Woo Ha, Sunghun Kim, and Jaegul Choo. 2018. StarGAN: Unified Generative Adversarial Networks for Multi-Domain Image-to-Image Translation. In *CVPR*.
- [3] Antonio Criminisi, Jamie Shotton, Andrew Blake, and Philip HS Torr. 2003. Gaze Manipulation for One-to-one Teleconferencing. In *ICCV*, Vol. 3. 13–16.
- [4] Brian Dolhansky and Cristian Canton Ferrer. 2018. Eye in-painting with exemplar generative adversarial networks. In *CVPR*. 7902–7911.
- [5] Kenneth Alberto Funes Mora, Florent Monay, and Jean-Marc Odobez. 2014. Eye-diap: A database for the development and evaluation of gaze estimation algorithms from rgb and rgb-d cameras. In *Proceedings of the Symposium on Eye Tracking Research and Applications*. 255–258.
- [6] Yaroslav Ganin, Daniil Kononenko, Diana Sungatullina, and Victor Lempitsky. 2016. Deepwarp: Photorealistic image resynthesis for gaze manipulation. In *ECCV*. Springer.
- [7] Ian Goodfellow, Jean Pouget-Abadie, Mehdi Mirza, Bing Xu, David Warde-Farley, Sherjil Ozair, Aaron Courville, and Yoshua Bengio. 2014. Generative adversarial nets. In *NIPS*.
- [8] Zhenliang He, Meina Kan, Jichao Zhang, and Shiguang Shan. 2020. PA-GAN: Progressive Attention Generative Adversarial Network for Facial Attribute Editing. *arXiv preprint arXiv:2007.05892* (2020).
- [9] Zhe He, Adrian Spurr, Xucong Zhang, and Otmar Hilliges. 2019. Photo-realistic monocular gaze redirection using generative adversarial networks. In *Proceedings of the IEEE International Conference on Computer Vision*. 6932–6941.
- [10] Zhenliang He, Wangmeng Zuo, Meina Kan, Shiguang Shan, and Xilin Chen. 2019. Attgan: Facial attribute editing by only changing what you want. *IEEE Transactions on Image Processing* 28, 11 (2019), 5464–5478.
- [11] Xun Huang, Ming-Yu Liu, Serge Belongie, and Jan Kautz. 2018. Multimodal unsupervised image-to-image translation. In *ECCV*. 172–189.
- [12] Satoshi Iizuka, Edgar Simo-Serra, and Hiroshi Ishikawa. 2017. Globally and Locally Consistent Image Completion. 36, 4, Article 107 (2017), 107:1–107:14 pages.
- [13] Satoshi Iizuka, Edgar Simo-Serra, and Hiroshi Ishikawa. 2017. Globally and locally consistent image completion. *TOG* 36, 4 (2017), 107.
- [14] Phillip Isola, Jun-Yan Zhu, Tinghui Zhou, and Alexei A Efros. 2017. Image-to-image translation with conditional adversarial networks. In *CVPR*.
- [15] Youngjoo Jo and Jongyoul Park. 2019. SC-FEGAN: Face Editing Generative Adversarial Network With User’s Sketch and Color. In *ICCV*.
- [16] Petr Kellnhofer, Adria Recasens, Simon Stent, Wojciech Matusik, and Antonio Torralba. 2019. Gaze360: Physically unconstrained gaze estimation in the wild. In *CVPR*.
- [17] Davis E King. 2009. Dlib-ml: A machine learning toolkit. *The Journal of Machine Learning Research* 10 (2009), 1755–1758.
- [18] R Kollarits, C Woodworth, J Ribera, and R Gitlin. 1996. 34.4: An eye contact camera/display system for videophone applications using a conventional direct-view LCD. In *Society for Information Display, International Symposium*. 765–768.
- [19] Daniil Kononenko, Yaroslav Ganin, Diana Sungatullina, and Victor Lempitsky. 2017. Photorealistic monocular gaze redirection using machine learning. *IEEE transactions on pattern analysis and machine intelligence* 40, 11 (2017), 2696–2710.
- [20] Daniil Kononenko and Victor Lempitsky. 2015. Learning to look up: Realtime monocular gaze correction using machine learning. In *CVPR*. 4667–4675.
- [21] Claudia Kuster, Tiberiu Popa, Jean-Charles Bazin, Craig Gotsman, and Markus Gross. 2012. Gaze correction for home video conferencing. *ACM Transactions on Graphics (TOG)* 31, 6 (2012), 174.
- [22] Christian Ledig, Lucas Theis, Ferenc Huszar, Jose Caballero, Andrew Cunningham, Alejandro Acosta, Andrew Aitken, Alykhan Tejani, Johannes Totz, Zehan Wang, and Wenzhe Shi. 2017. Photo-Realistic Single Image Super-Resolution Using a Generative Adversarial Network.
- [23] Hsin-Ying Lee, Hung-Yu Tseng, Jia-Bin Huang, Maneesh Kumar Singh, and Ming-Hsuan Yang. 2018. Diverse Image-to-Image Translation via Disentangled Representations. In *ECCV*.
- [24] Hongyu Liu, Bin Jiang, Yi Xiao, and Chao Yang. 2019. Coherent semantic attention for image inpainting. In *CVPR*.
- [25] Ming Liu, Yukang Ding, Min Xia, Xiao Liu, Errui Ding, Wangmeng Zuo, and Shilei Wen. 2019. STGAN: A unified selective transfer network for arbitrary image attribute editing. In *CVPR*. 3673–3682.
- [26] Si Liu, Yao Sun, Defa Zhu, Renda Bao, Wei Wang, Xiangbo Shu, and Shuicheng Yan. 2017. Face aging with contextual generative adversarial nets. In *ACMMM*.
- [27] Ziwei Liu, Ping Luo, Xiaogang Wang, and Xiaoou Tang. 2015. Deep learning face attributes in the wild. In *CVPR*.
- [28] Arun Mallya, Ting-Chun Wang, Karan Sapra, and Ming-Yu Liu. 2020. World-Consistent Video-to-Video Synthesis. *arXiv preprint arXiv:2007.08509* (2020).
- [29] Takeru Miyato, Toshiaki Kataoka, Masanori Koyama, and Yuichi Yoshida. 2018. Spectral normalization for generative adversarial networks. *arXiv preprint arXiv:1802.05957* (2018).
- [30] Ken-Ichi Okada, Fumihiko Maeda, Yusuke Ichikawa, and Yutaka Matsushita. 1994. Multiparty videoconferencing at virtual social distance: MAJIC design. In *Proceedings of the 1994 ACM conference on Computer supported cooperative work*. ACM, 385–393.
- [31] Kyle Olszewski, Duygu Ceylan, Jun Xing, Jose Echevarria, Zhili Chen, Weikai Chen, and Hao Li. 2020. Intuitive, Interactive Beard and Hair Synthesis with Generative Models. *arXiv preprint arXiv:2004.06848* (2020).
- [32] Seonwook Park, Shalini De Mello, Pavlo Molchanov, Umar Iqbal, Otmar Hilliges, and Jan Kautz. 2019. Few-shot adaptive gaze estimation. In *CVPR*. 9368–9377.
- [33] Taesung Park, Alexei A Efros, Richard Zhang, and Jun-Yan Zhu. 2020. Contrastive Learning for Unpaired Image-to-Image Translation. *arXiv preprint arXiv:2007.15651* (2020).
- [34] Taesung Park, Jun-Yan Zhu, Oliver Wang, Jingwan Lu, Eli Shechtman, Alexei A Efros, and Richard Zhang. 2020. Swapping Autoencoder for Deep Image Manipulation. *arXiv preprint arXiv:2007.00653* (2020).
- [35] Deepak Pathak, Philipp Krähenbühl, Jeff Donahue, Trevor Darrell, and Alexei Efros. 2016. Context Encoders: Feature Learning by Inpainting. In *CVPR*.
- [36] Deepak Pathak, Philipp Krähenbühl, Jeff Donahue, Trevor Darrell, and Alexei A Efros. 2016. Context encoders: Feature learning by inpainting. 2536–2544.
- [37] Brian A Smith, Qi Yin, Steven K Feiner, and Shree K Nayar. 2013. Gaze locking: passive eye contact detection for human-object interaction. In *Proceedings of the 26th annual ACM symposium on User interface software and technology*. 271–280.
- [38] Hao Tang, Song Bai, Li Zhang, Philip HS Torr, and Nicu Sebe. 2020. XingGAN for Person Image Generation. In *ECCV*.
- [39] Hao Tang, Dan Xu, Gaowen Liu, Wei Wang, Nicu Sebe, and Yan Yan. 2019. Cycle in cycle generative adversarial networks for keypoint-guided image generation. In *ACM MM*.
- [40] Hao Tang, Dan Xu, Nicu Sebe, Yanzhi Wang, Jason J. Corso, and Yan Yan. 2019. Multi-Channel Attention Selection GAN with Cascaded Semantic Guidance for Cross-View Image Translation. In *CVPR*.
- [41] Hao Tang, Dan Xu, Yan Yan, Philip HS Torr, and Nicu Sebe. 2020. Local Class-Specific and Global Image-Level Generative Adversarial Networks for Semantic-Guided Scene Generation. In *CVPR*.
- [42] Xintao Wang, Ke Yu, Shixiang Wu, Jinjin Gu, Yihao Liu, Chao Dong, Yu Qiao, and Chen Change Loy. 2018. ESRGAN: Enhanced super-resolution generative adversarial networks. In *ECCVW*.
- [43] Zhou Wang, Eero P Simoncelli, and Alan C Bovik. 2003. Multiscale structural similarity for image quality assessment. In *The Thirty-Seventh Asilomar Conference on Signals, Systems & Computers*, 2003, Vol. 2. Ieee.
- [44] Erroll Wood, Tadas Baltrušaitis, Louis-Philippe Morency, Peter Robinson, and Andreas Bulling. 2018. Gazedirector: Fully articulated eye gaze redirection in video. In *Computer Graphics Forum*, Vol. 37. Wiley Online Library, 217–225.
- [45] Po-Wei Wu, Yu-Jing Lin, Che-Han Chang, Edward Y Chang, and Shih-Wei Liao. 2019. Relgan: Multi-domain image-to-image translation via relative attributes. In *CVPR*. 5914–5922.
- [46] Ruigang Yang and Zhengyou Zhang. 2002. Eye gaze correction with stereovision for video-teleconferencing. In *ECCV*. Springer.
- [47] Ruigang Yang and Zhengyou Zhang. 2004. Eye gaze correction with stereovision for video-teleconferencing. *IEEE Transactions on Pattern Analysis and Machine Intelligence* 26, 7 (2004), 956–960.
- [48] Yu Yu, Gang Liu, and Jean-Marc Odobez. 2019. Improving few-shot user-specific gaze adaptation via gaze redirection synthesis. In *CVPR*.
- [49] Gang Zhang, Meina Kan, Shiguang Shan, and Xilin Chen. 2018. Generative adversarial network with spatial attention for face attribute editing. In *ECCV*. 417–432.
- [50] Haoran Zhang, Zhenzhen Hu, Changzhi Luo, Wangmeng Zuo, and Meng Wang. 2018. Semantic image inpainting with progressive generative networks. In *ACMMM*.
- [51] Jichao Zhang, Yezhi Shu, Songhua Xu, Gongze Cao, Fan Zhong, Meng Liu, and Xueying Qin. 2018. Sparsely Grouped Multi-Task Generative Adversarial Networks for Facial Attribute Manipulation. In *Proceedings of the 26th ACM International Conference on Multimedia* (Seoul, Republic of Korea) (MM ’18). ACM, New York, NY, USA, 392–401. <https://doi.org/10.1145/3240508.3240594>
- [52] Richard Zhang, Phillip Isola, Alexei A Efros, Eli Shechtman, and Oliver Wang. 2018. The Unreasonable Effectiveness of Deep Features as a Perceptual Metric. In *CVPR*.
- [53] Xucong Zhang, Seonwook Park, Thabo Beeler, Derek Bradley, Siyu Tang, and Otmar Hilliges. 2020. ETH-XGaze: A Large Scale Dataset for Gaze Estimation under Extreme Head Pose and Gaze Variation. *arXiv preprint arXiv:2007.15837* (2020).
- [54] Xucong Zhang, Yusuke Sugano, Mario Fritz, and Andreas Bulling. 2017. Mpiigaze: Real-world dataset and deep appearance-based gaze estimation. *IEEE transactions on pattern analysis and machine intelligence* 41, 1 (2017), 162–175.
- [55] Jun-Yan Zhu, Taesung Park, Phillip Isola, and Alexei A. Efros. 2017. Unpaired Image-To-Image Translation Using Cycle-Consistent Adversarial Networks.

Module	Input Shape	Layer Information
Global D	$(h, w, 3)$	Input
	$(h, w, 3)$	CONV-(C32 K4×4, S2×2), LReLU
	$(\frac{h}{2}, \frac{w}{2}, 32)$	CONV-(C64 K4×4, S2×2), LReLU
	$(\frac{h}{4}, \frac{w}{4}, 64)$	CONV-(C128 K4×4, S2×2), LReLU
	$(\frac{h}{8}, \frac{w}{8}, 128)$	CONV-(C256 K4×4, S2×2), LReLU
	$(\frac{h}{16}, \frac{w}{16}, 256)$	CONV-(C256 K4×4, S2×2), LReLU
	$(\frac{h}{32}, \frac{w}{32}, 256)$	CONV-(C256 K4×4, S2×2), LReLU
	$(\frac{h}{64}, \frac{w}{64}, 256)$	FC-(C256)
Local D	$(\frac{h}{2}, \frac{w}{2}, 3)$	Input
	$(\frac{h}{2}, \frac{w}{2}, 3)$	CONV-(C32 K4×4, S2×2), LReLU
	$(\frac{h}{4}, \frac{w}{4}, 32)$	CONV-(C64 K4×4, S2×2), LReLU
	$(\frac{h}{8}, \frac{w}{8}, 64)$	CONV-(C128 K4×4, S2×2), LReLU
	$(\frac{h}{16}, \frac{w}{16}, 128)$	CONV-(C256 K4×4, S2×2), LReLU
	$(\frac{h}{32}, \frac{w}{32}, 256)$	CONV-(C256 K4×4, S2×2), LReLU
	$(\frac{h}{64}, \frac{w}{64}, 256)$	CONV-(C256 K4×4, S2×2), LReLU
	$(\frac{h}{128}, \frac{w}{128}, 256)$	FC-(C256)
Concat	(512)	FC-(C512), LReLU
	(512)	FC-(C1)

Table 5: The architectures of global and local discriminator D_x and D_y . Both have the same architecture.

Module	Input Shape	Layer Information
Encoder	$(h, w, 3 + 1)$	Input
	$(h, w, 4)$	CONV-(C16, K7×7, S1×1), IN, LReLU
	$(h, w, 16)$	CONV-(C32, K4×4, S2×2), IN, LReLU
	$(\frac{h}{2}, \frac{w}{2}, 32)$	CONV-(C64, K4×4, S2×2), IN, LReLU
	$(\frac{h}{4}, \frac{w}{4}, 64)$	CONV-(C128, K4×4, S2×2), IN, LReLU
	$(\frac{h}{8}, \frac{w}{8}, 128)$	CONV-(C256, K4×4, S2×2), IN, LReLU
	$(\frac{h}{16}, \frac{w}{16}, 256)$	CONV-(C256, K4×4, S2×2), IN, LReLU
	$(\frac{h}{32}, \frac{w}{32}, 128)$	FC-(C256)
Decoder	(256)	FC-(C256 × $\frac{h}{32} \times \frac{w}{32}$)
	$(\frac{h}{32}, \frac{w}{32}, 256)$	DECONV-(C128, K4×4, S2×2), IN, LReLU
	$(\frac{h}{16}, \frac{w}{16}, 128)$	DECONV-(C64, K4×4, S2×2), IN, LReLU
	$(\frac{h}{8}, \frac{w}{8}, 64)$	DECONV-(C32, K4×4, S2×2), IN, LReLU
	$(\frac{h}{4}, \frac{w}{4}, 32)$	DECONV-(C16, K4×4, S2×2), IN, LReLU
	$(\frac{h}{2}, \frac{w}{2}, 16)$	DECONV-(C16, K4×4, S2×2), IN, LReLU
	$(h, w, 16)$	CONV-(C3, K7×7, S1×1), Tanh

Table 6: The architectures of Encoder and Decoder in generator G_x . The mask M would be also as input of G_x .

C GAZE CORRECTION.



Figure 10: More comparison results for gaze correction in test data from domain Y . We can find GazeGAN achieves more realistic results with precise gaze angle than the base-lines.

D CELEBAGAZE DATASET.

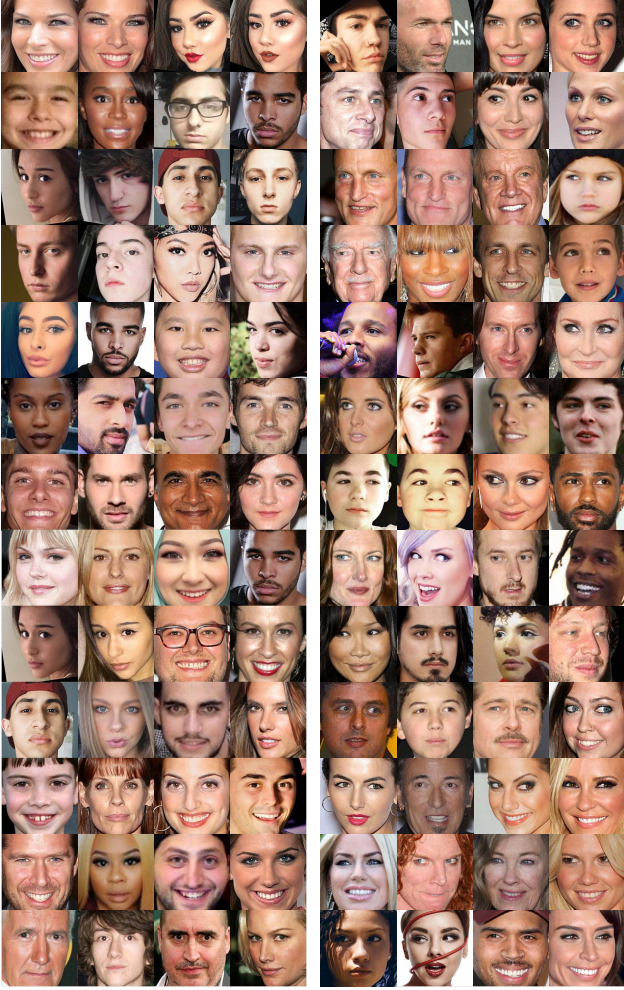


Figure 11: More examples from our CelebAGaze dataset. Left is from domain X with staring at the cameras for gaze. Right is from domain Y with staring at somewhere else for gaze.

Module	Input Shape	Layer Information
Encoder	$(\frac{h}{2}, \frac{w}{2}, 3)$	CONV-(C16, K7×7, S1×1), IN, LReLU
	$(\frac{h}{2}, \frac{w}{2}, 16)$	CONV-(C32, K4×4, S2×2), IN, LReLU
	$(\frac{h}{4}, \frac{w}{4}, 32)$	CONV-(C64, K4×4, S2×2), IN, LReLU
	$(\frac{h}{8}, \frac{w}{8}, 64)$	CONV-(C128, K4×4, S2×2), IN, LReLU
	$(\frac{h}{16}, \frac{w}{16}, 128)$	FC-(C256)
Decoder	$(\frac{h}{16}, \frac{w}{16}, 256)$	DECONV-(C128, K4×4, S2×2), IN, LReLU
	$(\frac{h}{8}, \frac{w}{8}, 128)$	DECONV-(C64, K4×4, S2×2), IN, LReLU
	$(\frac{h}{4}, \frac{w}{4}, 64)$	DECONV-(C32, K4×4, S2×2), IN, LReLU
	$(\frac{h}{2}, \frac{w}{2}, 16)$	CONV-(C3, K7×7, S1×1), Tanh

Table 7: The architectures of the proposed self-supervised eye-flipping autoencoder G_{pre} . And it will be pretrained first.

A INTRODUCTION

This supplementary document provides additional results supporting the claims of the main paper.

Firstly, we show the network architecture of G_x , G_y , D and G_{pre} in Table 6, Table 4, Table 5 and Table 7. Note that D_x and D_y have the same architecture D . Secondly, we show more examples of CelebAGaze dataset in Fig. 11. Finally, Fig. 10 and Fig. 12 show more gaze correction and animation results by interpolation in latent space to validate the effectiveness and superiority of GazeGAN.

B NETWORK ARCHITECTURE

Here are some notations should be noted: CONV: convolutional layer; DECONV: deconvolutional layer. h : height of input images; w : width of the input images; C: number of output channels; K: size of kernels; S: strides of kernels; IN: instance normalization; LReLU: Leaky ReLU; In our experiments, $h = 256$, $w = 256$.

Module	Input Shape	Layer Information
Encoder	$(h, w, 3 + 1)$	Input
	$(h, w, 4)$	CONV-(C16, K7×7, S1×1), IN, LReLU
	$(h, w, 16)$	CONV-(C32, K4×4, S2×2), IN, LReLU
	$(\frac{h}{2}, \frac{w}{2}, 32)$	CONV-(C64, K4×4, S2×2), IN, LReLU
	$(\frac{h}{4}, \frac{w}{4}, 64)$	CONV-(C128, K4×4, S2×2), IN, LReLU
	$(\frac{h}{8}, \frac{w}{8}, 128)$	CONV-(C256, K4×4, S2×2), IN, LReLU
	$(\frac{h}{16}, \frac{w}{16}, 256)$	CONV-(C256, K4×4, S2×2), IN, LReLU
Encoder E_r	$(\frac{h}{2}, \frac{w}{2}, 3)$	Input
	$(\frac{h}{2}, \frac{w}{2}, 3)$	CONV-(C32, K7×7, S1×1), IN, LReLU
	$(\frac{h}{2}, \frac{w}{2}, 32)$	CONV-(C64, K4×4, S2×2), IN, LReLU
	$(\frac{h}{4}, \frac{w}{4}, 64)$	CONV-(C128, K4×4, S2×2), IN, LReLU
	$(\frac{h}{8}, \frac{w}{8}, 128)$	CONV-(C128, K4×4, S2×2), IN, LReLU
	$(\frac{h}{16}, \frac{w}{16}, 128)$	FC-(C2)
Decoder	(258)	FC-(C256 × $\frac{h}{32} \times \frac{w}{32}$)
	$(\frac{h}{32}, \frac{w}{32}, 256)$	DECONV-(C128, K4×4, S2×2), IN, LReLU
	$(\frac{h}{16}, \frac{w}{16}, 128)$	DECONV-(C64, K4×4, S2×2), IN, LReLU
	$(\frac{h}{8}, \frac{w}{8}, 64)$	DECONV-(C32, K4×4, S2×2), IN, LReLU
	$(\frac{h}{4}, \frac{w}{4}, 32)$	DECONV-(C16, K4×4, S2×2), IN, LReLU
	$(\frac{h}{2}, \frac{w}{2}, 16)$	DECONV-(C16, K4×4, S2×2), IN, LReLU
	$(h, w, 16)$	CONV-(C3, K7×7, S1×1), Tanh

Table 4: The architectures of Encoder and Decoder in generator G_y . The mask M would be also as input of G_y .

E GAZE ANIMATION.

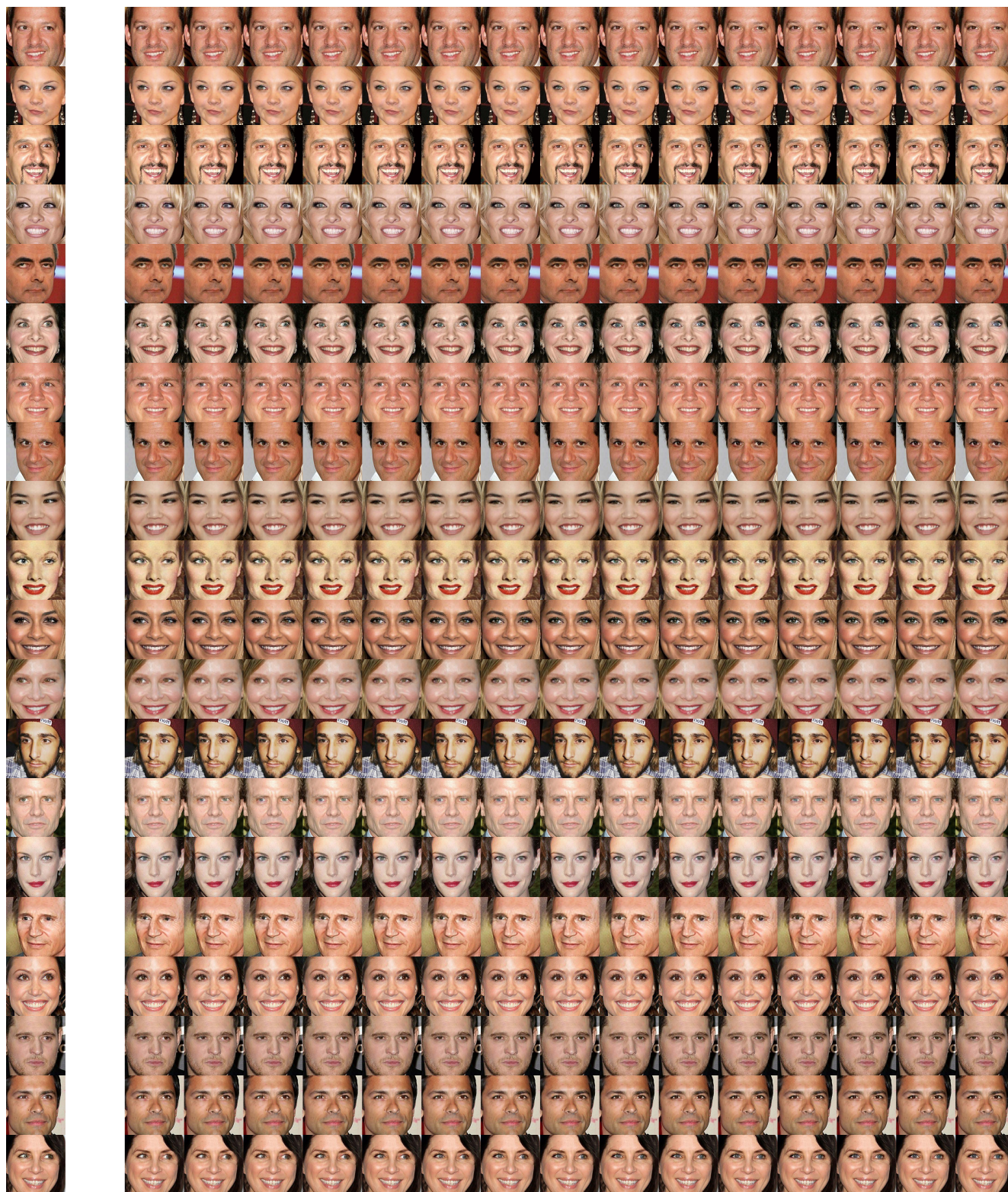


Figure 12: More gaze animation results in the wild.